Int. J. Solids Structures Vol. 30, No. 4, pp. 483–498, 1993
Printed in Great Britain

0020–7683/93 $5.00+ .00

STEADY-STATE MODE III PROPAGATION OF AN INTERFACE CRACK IN AN INHOMOGENEOUS VISCOELASTIC STRIP

MICHAEL RYVKIN and LESLIE BANKS-SILLS
Department of Solid Mechanics, Materials and Structures, Faculty of Engineering,
Tel Aviv University, 69978 Ramat Aviv, Israel

(*Received* 29 *April* 1992; *in revised form* 24 *August* 1992)

Abstract—The problem of a steady propagating semi-infinite crack between two bonded, viscoelastic infinite strips subjected to mode III deformation is investigated. A Wiener–Hopf equation is formulated and solved in closed form by means of a Cauchy-type integral. The integral is evaluated yielding the stress intensity factor for various material combinations including a homogeneous Maxwell material, two bonded Maxwell materials, a bonded elastic and Maxwell material and two standard solids. The correspondence principle is employed to obtain the stress intensity factor value for a standing crack (i.e. $v = 0$). Results are presented in graphical form for some cases of interest.

1. INTRODUCTION

An important aspect of damage of composite materials is the initiation and propagation of cracks along the interface between layers possessing different material properties. The purpose of this work is to investigate the steady propagation of a semi-infinite crack between two infinite strips of viscoelastic material which are subjected to mode III deformation. This same problem in the case of two elastic materials was considered by Matczynski (1974); for various boundary conditions, the crack tip stress and displacement jump, and the stress intensity factor were determined. Sills and Benveniste (1981) and Banks-Sills and Benveniste (1983) determined the mode III stress intensity factor for a crack propagating steadily between two different viscoelastic half-spaces where the media were modeled as Maxwell materials and standard solids, respectively. Later, Coussy (1987) determined the long and short time behavior for a suddenly appearing crack in the same geometry subjected to mode III deformation. In addition, a homogeneous viscoelastic strip containing a semi-infinite symmetric crack, subjected to mode III deformation was investigated by Atkinson and Popelar (1979) and Walton (1985). Atkinson and Popelar (1979) formulated the transient problem for a general viscoelastic solid and then determined the stress intensity factor and energy release rate for steady propagation. Graphical results were presented for a standard solid. Walton (1985) reconsidered the steady problem for a more general viscoelastic material and two sets of boundary conditions.

In this study, both Maxwell materials and standard solids are considered. As with previous investigations, the mathematical technique which is employed in this investigation consists of the application of a Fourier transform and the solution of a resulting Wiener–Hopf equation. The mathematical analysis for each material pair is presented in Section 2. Closed form solutions for the stress intensity factor are determined. Factorization of the complex valued function in the Wiener–Hopf equation is carried out by means of Cauchy-type integrals along the real axis. In Section 3, results are presented for various material combinations including an elastic layer laminated to a Maxwell material and two standard solids. In each case, results for a standing crack are obtained by means of the correspondence principle and are seen to agree with the behavior of the solution as the crack velocity v, approaches zero.

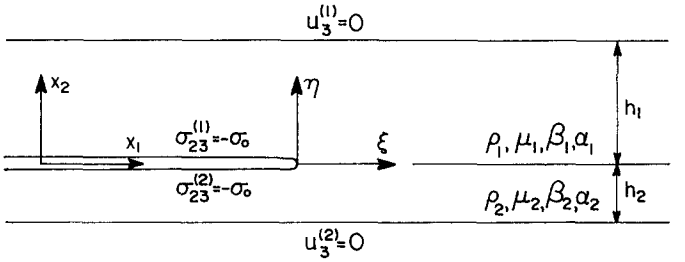

Fig. 1. An interface crack in an inhomogeneous, viscoelastic strip.

2. ANALYSIS

Consider a semi-infinite crack between two viscoelastic bonded strips with a fixed coordinate system (x_1, x_2, x_3) defined with $x_2 = 0$ being the interface of the media (Fig. 1). Since mode III behavior is to be investigated, the crack faces are subjected to the shear stresses

$$\sigma_{23}^{(r)}(x_1, 0, x_3, t) = -\sigma_0, \quad x_1 - vt < 0 \tag{1}$$

and the displacements are restrained at the outer strip boundaries, so that

$$u_3^{(r)}(x_1, (-1)^{r-1}h_r, x_3, t) = 0, \tag{2}$$

where $r = 1, 2$ denote the upper and lower medium respectively, t represents time, σ_0 is a constant with dimensions of stress, and h_r are the respective thicknesses of the upper and lower strips.

As seen from these equations, the applied tractions and displacements are independent of x_3, thus an anti-plane strain motion results with displacements being given as

$$u_1^{(r)} = u_2^{(r)} \equiv 0, \quad u_3^{(r)} \equiv w^{(r)}(x_1, x_2, t). \tag{3}$$

According to (3), the non-vanishing strains are given by

$$\varepsilon_{\omega 3}^{(r)} = \frac{1}{2}\frac{\partial w^{(r)}}{\partial x_\omega}, \tag{4}$$

with $\omega = 1, 2$.

The viscoelastic material behavior of both materials is modeled as a standard solid. For each medium, the constitutive equations for the non-zero stresses may be written as

$$\frac{\partial \sigma_{\omega 3}^{(r)}}{\partial t} + \beta_r \sigma_{\omega 3}^{(r)} = 2\mu_r\left(\frac{\partial \varepsilon_{\omega 3}^{(r)}}{\partial t} + \alpha_r \varepsilon_{\omega 3}^{(r)}\right), \tag{5}$$

where $1/\beta_r$ and $1/\alpha_r$ are the relaxation and creep times respectively, μ_r and $\mu_r^* = (\alpha_r/\beta_r)\mu_r$ are the instantaneous short time and long time moduli, respectively. To examine a Maxwell material as well, the creep times become infinite so that α_r is taken to be zero.

For the considered anti-plane strain deformation, the equation of motion in each material is given by

$$\frac{\partial \sigma_{13}^{(r)}}{\partial x_1} + \frac{\partial \sigma_{23}^{(r)}}{\partial x_2} = \rho_r \frac{\partial^2 w^{(r)}}{\partial t^2}, \tag{6}$$

where ρ_r denotes density. The continuity conditions to be satisfied along the interface are

and
$$\left.\begin{aligned}\sigma_{23}^{(1)}(x_1,0,t) &= \sigma_{23}^{(2)}(x_1,0,t)\\ w^{(1)}(x_1,0,t) &= w^{(2)}(x_1,0,t)\end{aligned}\right\} \quad x_1-vt>0. \tag{7}$$

Next, it is convenient to define a moving Galilean coordinate system (ξ,η) whose origin coincides with the crack tip and whose axes are parallel to the fixed (x_1,x_2) axes respectively (see Fig. 1). Hence

$$\xi = x_1-vt, \quad \eta = x_2. \tag{8}$$

Since steady-state motion is to be investigated, this condition together with relations (8) imply that

$$\frac{\partial}{\partial x_1}=\frac{\partial}{\partial \xi}, \quad \frac{\partial}{\partial x_2}=\frac{\partial}{\partial \eta}, \quad \frac{\partial}{\partial t}=-v\frac{\partial}{\partial \xi}. \tag{9}$$

The partial differential equations (5) and (6) in the moving frame may be reduced to ordinary differential equations by application of a Fourier transform in ξ defined as

$$\bar{f}(s,\eta)=\int_{-\infty}^{\infty} f(\xi,\eta)\exp(is\xi)\,\mathrm{d}\xi,$$

where s is a complex variable. The constitutive equations (5) for each medium become

and
$$\begin{aligned}(s-i\beta_r/v)\bar{\sigma}_{13}^{(r)} &= -i\mu_r s(s-i\alpha_r/v)\bar{w}^{(r)}\\ (s-i\beta_r/v)\bar{\sigma}_{23}^{(r)} &= \mu_r(s-i\alpha_r/v)\frac{\mathrm{d}\bar{w}^{(r)}}{\mathrm{d}\eta};\end{aligned} \tag{10}$$

the equations of motion (6) transform into

$$-is\bar{\sigma}_{13}^{(r)}+\frac{\mathrm{d}\bar{\sigma}_{23}^{(r)}}{\mathrm{d}\eta}=-v^2\rho_r s^2\bar{w}^{(r)}. \tag{11}$$

Substitution of the transformed stresses from (10) into (11) yields

$$\frac{\mathrm{d}^2\bar{w}^{(r)}}{\mathrm{d}\eta^2}-\gamma_r^2\bar{w}^{(r)}=0, \tag{12}$$

where

$$\gamma_r^2=s^2\left(s-\frac{i\alpha_r}{v}\right)^{-1}\left[\left(1-\frac{v^2}{c_r^2}\right)s-i\left(1-\frac{v^2}{c_r^{*2}}\right)\frac{\alpha_r}{v}\right]. \tag{13}$$

The short and long time wave speeds are respectively $c_r^2=\mu_r/\rho_r$ and $c_r^{*2}=\alpha_r c_r^2/\beta_r=\mu_r^*/\rho_r$. It is convenient to choose the branches of γ_r so that $\mathrm{Re}(\gamma_r)>0$.

The general solution of eqn (12) is given by

$$\bar{w}^{(r)}(s,\eta)=E_r(s)\sinh(\gamma_r\eta)+F_r(s)\cosh(\gamma_r\eta). \tag{14}$$

From the boundary condition (2), it may be shown that

$$\bar{w}^{(r)}(s,\eta)=E_r(s)\frac{\sinh[\gamma_r(\eta-(-1)^{r-1}h_r)]}{\cosh(\gamma_r h_r)}. \tag{15}$$

In order to form the Wiener–Hopf problem, (15) must be used in conjunction with the

Fourier transformations of the boundary and continuity conditions (1) and (7). Following Sills and Benveniste (1981), the problem may be reduced to one Wiener–Hopf equation given by

$$W^-(s) = -P(s)H^+(s) - \frac{i\sigma_0}{s}P(s), \quad s \in L, \tag{16}$$

where the contour L is located in the lower half s-plane near the real axis $\{L: \mathrm{Im}(s) = -\varepsilon, \varepsilon > 0\}$. $W^-(s)$ represents the Fourier transform of the unknown displacement jump across the crack faces in the complex variable space, namely

$$W^-(s) = \int_{-\infty}^{0} [w^{(1)}(\xi, 0) - w^{(2)}(\xi, 0)] \exp(is\xi)\, d\xi \tag{17}$$

and is analytic in a lower half plane. $H^+(s)$ is the Fourier transform of the continuous unknown stress $\sigma_{23}^{(r)}$ along the strip interface given by

$$H^+(s) = \int_0^{\infty} \sigma_{23}^{(r)}(\xi, 0) \exp(is\xi)\, d\xi \tag{18}$$

which is analytic in an upper half plane. The function $P(s)$ is given by

$$P(s) = \frac{s - i\beta_1/v}{s - i\alpha_1/v} \frac{\tanh(\gamma_1 h_1)}{\mu_1 \gamma_1} + \frac{s - i\beta_2/v}{s - i\alpha_2/v} \frac{\tanh(\gamma_2 h_2)}{\mu_2 \gamma_2}. \tag{19}$$

It is interesting to note that in contrast to the analogous infinite space problem (Sills and Benveniste, 1981; Banks-Sills and Benveniste, 1983), here, the function $P(s)$ is meromorphic. This may be easily verified from eqns (13) and (19) by expanding the functions $\tanh(\gamma_r h_r)$ in a Taylor series of their arguments, showing $P(s)$ to be only a function of $\gamma_r^2(s)$ and multiplying polynomials.

In order to solve eqn (16), the function $P(s)$ must be factored into two functions $P^+(s)$ and $P^-(s)$ such that each is analytic and non-zero in some upper and lower half plane, respectively. To this end, $P(s)$ is rewritten as the product of two functions

$$P(s) = F_1(s)F_2(s), \tag{20}$$

where

$$F_i(s) = \frac{F_i^+(s)}{F_i^-(s)}, \quad s \in L, \tag{21}$$

$i = 1, 2$. Equation (21) may be viewed as two Riemann boundary value problems. Employing the theory of these problems, the function $F_2(s)$ is chosen so that it may be factored as the exponential of a Cauchy-type integral, namely

$$F_2^{\pm}(s) = \exp\left\{\frac{1}{2\pi i}\int_L \frac{\ln F_2(t)}{t - s}\, dt\right\} \tag{22}$$

and so that $F_1(s)$ may be factored by inspection. The representation in (22) may be written when $F_2(s)$ satisfies the following conditions on L:

(a) $F_2(s)$ is Hölder continuous,

(b) $\lim_{\mathrm{Re}(s) \to \pm\infty} F_2(s) = 1$,

(c) the index of $F_2(s)$ on L is zero.

For a detailed discussion of these conditions and the general theory of Riemann boundary value problems see Gakhov (1966). Thus, from (20) and (21), the factorization of $P(s)$ may be written as

$$P^{\pm}(s) = F_1^{\pm}(s)F_2^{\pm}(s). \tag{23}$$

Assuming that $P(s)$ may be factored as in eqn (23), the Wiener–Hopf equation in (16) may be rearranged as

$$P^{+}(s)\left[\frac{i\sigma_0}{s} + H^{+}(s)\right] = -W^{-}(s)P^{-}(s), \quad s \in L. \tag{24}$$

Next, the term $i\sigma_0 P^{+}(s)/s$ is written as the sum of a plus and minus function so that (24) becomes

$$P^{+}(s)H^{+}(s) + \frac{i\sigma_0}{s}[P^{+}(s) - P^{+}(0)] = -W^{-}(s)P^{-}(s) - \frac{i\sigma_0}{s}P^{+}(0), \quad s \in L. \tag{25}$$

In order to solve eqn (25) for the unknown transformed stress $H^{+}(s)$ and displacement jump $W^{-}(s)$, explicit expressions for $P^{+}(s)$ and $P^{-}(s)$ must be found. To this end, in Subsections 2.1 and 2.2 a Maxwell material and standard solid are treated separately.

2.1. *Maxwell material*

The factorization and solution is first carried out for two Maxwell materials. In this case, $\alpha_r = 0$, so that from eqn (13)

$$\gamma_r^2 = s(a_r^2 s + i\beta_r v/c_r^2), \tag{26}$$

where

$$a_r^2 = 1 - v^2/c_r^2 \tag{27}$$

and from (19)

$$P(s) = \frac{s - i\beta_1/v}{s}\frac{\tanh(\gamma_1 h_1)}{\mu_1\gamma_1} + \frac{s - i\beta_2/v}{s}\frac{\tanh(\gamma_2 h_2)}{\mu_2\gamma_2}. \tag{28}$$

In order to satisfy the conditions mentioned above for the factorization of $F_2(s)$, we choose

$$F_2(s) = \frac{\sqrt{s^2+1}}{Q(\infty)}\left(\frac{\tanh(\gamma_1 h_1)}{\mu_1\gamma_1} + \frac{s - i\beta_2/v}{s - i\beta_1/v}\frac{\tanh(\gamma_2 h_2)}{\mu_2\gamma_2}\right) \tag{29}$$

so that

$$F_1(s) = \frac{s - i\beta_1/v}{s}\frac{Q(\infty)}{\sqrt{s^2+1}}, \tag{30}$$

where

$$Q(s) = \frac{s\sqrt{s^2+1}}{s - i\beta_1/v}P(s).$$

Note that it is possible to rewrite $F_2(s)$ as

$$F_2(s) = \frac{Q(s)}{Q(\infty)}. \tag{31}$$

Since

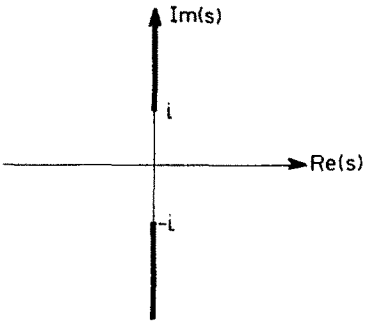

Fig. 2. Branch cuts in the s-plane for the functions $\sqrt{s+i}$ and $\sqrt{s-i}$.

$$Q(\infty) = \lim_{\mathrm{Re}\,(s)\to\infty} Q(s),$$

$$Q(\infty) = \frac{1}{\mu_1 a_1} + \frac{1}{\mu_2 a_2}. \tag{32}$$

By observation $F_1(s)$ may be factored as

$$F_1^+(s) = \left(\frac{Q(\infty)}{s+i}\right)^{1/2} \tag{33}$$

and

$$F_1^-(s) = \left(\frac{s-i}{Q(\infty)}\right)^{1/2} \frac{s}{s-i\beta_1/v}. \tag{34}$$

The branch for each square root in (33) and (34) is chosen with positive real part for $\mathrm{Im}\,(s) = 0$; the branch cuts are shown in Fig. 2.

In order to carry out the integration in eqn (22) for the factorization of $F_2(s)$, conditions (a)–(c) must be satisfied. Conditions (a) and (b) can be easily fulfilled employing eqns (26), (29) and (32). Verification of condition (c) is presented in the Appendix. Thus, explicit expressions exist for $F_i^{\pm}(s)$, $i = 1, 2$, and therefore for $P^{\pm}(s)$.

It is now possible to obtain the solution of the Wiener–Hopf equation in (25). Functions on the left- and right-hand sides are analytic in upper and lower half planes, respectively, and equal on the contour L. Under these conditions, the principle of analytic continuation states that each represents an entire function $M(s)$ in their respective half planes. Furthermore, from physical consideration of the behavior of the stress and the displacement jump near the crack tip, it is possible to conclude that $H^+(s) = O(s^{-1/2})$ and $W^-(s) = O(s^{-3/2})$ as $|s| \to \infty$. In addition, from eqn (23), $P^{\pm}(s) = O(s^{\mp 1/2})$ as $|s| \to \infty$. Thus, the left-hand side of (25) tends to zero as $|s| \to \infty$, $\mathrm{Im}\,(s) \geqslant -\varepsilon$, and the right-hand side of (25) tends to zero as $|s| \to \infty$, $\mathrm{Im}\,(s) \leqslant -\varepsilon$. It may then be concluded by Liouville's theorem that $M(s) \equiv 0$ and, therefore

$$H^+(s) = \frac{i\sigma_0}{s}\left[\frac{P^+(0)}{P^+(s)} - 1\right] \tag{35}$$

and

$$W^-(s) = -\frac{i\sigma_0}{s}\frac{P^+(0)}{P^-(s)}. \tag{36}$$

By applying the Fourier inverse transform to these quantities along the contour L, it is

possible to obtain expressions for stresses and displacements on the material interface, as well as at all points within the strip.

Since it is the stress intensity factor which is of prime importance, it is sufficient to determine an expression for the stress $\sigma_{23}(\xi, 0)$ as $\xi \to 0^+$ or equivalently its transform $H^+(s)$ as $|s| \to \infty$. From (22), (23), (33) and (35), the asymptotic behavior of the stress transform $H^+(s)$ is found to be

$$H^+(s) \sim \frac{\sigma_0}{\sqrt{s}} \exp\left(i\frac{\pi}{4}\right) F_2^+(0), \quad |s| \to \infty. \tag{37}$$

Applying Abelian type theorems found in Noble (1958), one obtains

$$\sigma_{23}^{(r)}(\xi^+, 0) \sim \frac{\sigma_0}{\sqrt{\pi\xi}} F_2^+(0), \quad \xi \to 0. \tag{38}$$

In calculating $F_2^+(0)$ from (22), it is convenient to move the integration path L to the real axis, which will be denoted further as L_1. Because of the regularity and absence of zeros of $F_2(s)$ in the domain $-\varepsilon \leqslant \operatorname{Im}(s) \leqslant 0$, as mentioned in the Appendix, translation of contour L to the real axis is justified. Applying the Plemelj formulas, one can obtain from (22) and (29)

$$F_2^+(0) = \left[\frac{Q(0)}{Q(\infty)}\right]^{1/2} \exp(J), \tag{39}$$

where

$$J = \frac{1}{\pi}\int_0^\infty \frac{\arg F_2(t)}{t}\,dt. \tag{40}$$

The symmetry of $F_2(\tau)$ according to (A1) has been employed in writing the integral in (40). The integrand in (40) is not singular at $t = 0$; for $t \to \infty$, it decays algebraically as $O(t^{-2})$. Thus, there are no serious difficulties in performing the integration numerically.

The non-dimensional viscoelastic stress intensity factor is defined as

$$\hat{K}_{ve} = \frac{1}{K_e}\lim_{\xi \to 0^+} \sqrt{2\pi\xi}\,\sigma_{23}(\xi, 0), \tag{41}$$

where

$$K_e = \sigma_0\left[\frac{h_1\mu_2 + h_2\mu_1}{\mu_1 + \mu_2}\right]^{1/2}. \tag{42}$$

Note that, K_e is the stress intensity factor for a standing crack ($v = 0$) in an elastic, inhomogeneous strip [see Matczynski (1974)]. Substituting (38) and (42) into (41) yields the non-dimensional stress intensity factor of a crack propagating steadily along the interface of two viscoelastic Maxwell materials in mode III

$$\hat{K}_{ve} = \left[\frac{\mu_1 + \mu_2}{h_1\mu_2 + h_2\mu_1}\frac{Q(0)}{Q(\infty)}\right]^{1/2} \exp(J). \tag{43}$$

In (43), $Q(0)$, $Q(\infty)$ and J are given by (A3), (32) and (40), respectively.

2.2. *Standard solid*

The solution for two standard solids may be obtained with some changes in the previous analysis for the Maxwell materials. In this case, α_r are non-zero, so that γ_r and

$P(s)$ are given in eqns (13) and (19), respectively. The function $F_2(s)$ is defined by eqn (31) with $Q(s)$ chosen as

$$Q(s) = \sqrt{s^2+1}P(s); \tag{44}$$

so that

$$F_2(s) = \frac{\sqrt{s^2+1}}{Q(\infty)}\left(\psi_1(s)\frac{\tanh(\gamma_1 h_1)}{\mu_1\gamma_1} + \psi_2(s)\frac{\tanh(\gamma_2 h_2)}{\mu_2\gamma_2}\right), \tag{45}$$

where

$$\psi_r(s) = \frac{s - i\beta_r/v}{s - i\alpha_r/v} \tag{46}$$

and

$$F_1(s) = \frac{Q(\infty)}{\sqrt{s^2+1}}. \tag{47}$$

The factorization of $F_1(s)$ is given by

$$F_1^{\pm}(s) = \left(\frac{Q(\infty)}{s \pm i}\right)^{1/2}. \tag{48}$$

To employ the integral in (22) for factoring $F_2(s)$, conditions (a)–(c) must be re-examined and satisifed. Conditions (a) and (b) may be verified by observation; condition (c) is verified in the Appendix.

Next, to solve the Wiener–Hopf equation in (25), the asymptotic behavior of the functions $P^{\pm}(s)$ is required. It is easy to show from (22), (23) and (48) that the behavior of these two functions is the same as for that of a Maxwell material. All relations from (35) through (43) for the Maxwell material remain valid. In the expression for the viscoelastic stress intensity factor, namely (43), $Q(0)$ from (A3) is replaced by

$$Q(0) = \frac{h_1}{\mu_1^*} + \frac{h_1}{\mu_2^*}, \tag{49}$$

where it may be recalled that $\mu_r^* = (\alpha_r/\beta_r)\mu_r$.

3. RESULTS

In this section, graphs are presented in Figs 3–7 illustrating the behavior of the stress intensity factor as a function of crack-tip velocity for specific material combinations.

3.1. *Maxwell material*

For a Maxwell material, the non-dimensional stress intensity factor $\hat{K}_{ve}$ defined in (41) is seen to be a function of several non-dimensional parameters, namely

$$\hat{K}_{ve} = \hat{K}_{ve}[v/\min(c_1, c_2); \beta_2/\beta_1, \beta_1 h_1/c_1, h_2/h_1, c_2/c_1, \mu_2/\mu_1]. \tag{50}$$

The parameter $\beta_1 h_1/c_1$ may be viewed as the ratio of the time h_1/c_1 required for a shear wave to traverse the upper material thickness to the material relaxation time $1/\beta_1$.

Before describing specific results, the values of $\hat{K}_{ve}$ for crack-tip velocity v, zero and $\min(c_1, c_2)$ are considered. At $v = 0$, this value is defined as

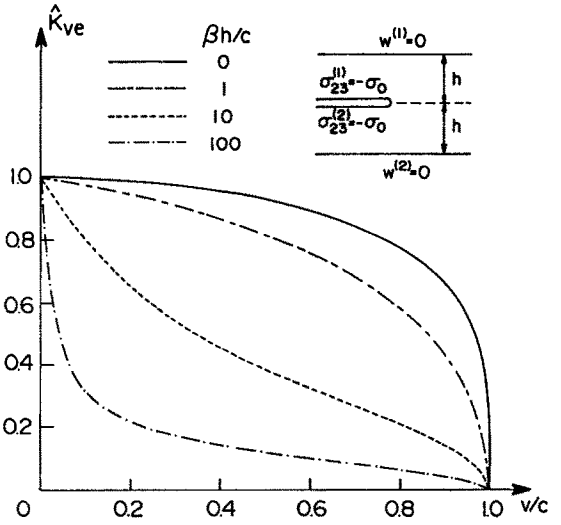

Fig. 3. Graph of the non-dimensional stress intensity factor $\hat{K}_{ve}$ vs the non-dimensional crack-tip velocity v/c for homogeneous viscoelastic (Maxwell material) strips containing a symmetrical crack ($h_2/h_1 = 1$) with $\mu_2/\mu_1 = 1$, $c_2/c_1 = 1$ and $\beta_2/\beta_1 = 1$. Also shown is the curve for a homogeneous elastic material, $\beta h/c = 0$.

$$\hat{K}_{ve}^0 = \lim_{v \to 0} \hat{K}_{ve}. \tag{51}$$

Since the transformation in (9) breaks down for $v = 0$, the solution degenerates at this point making it impossible to obtain $\hat{K}_{ve}^0$ directly from the expression in (43). Instead, the correspondence principle for viscoelastic materials [see for example, Christensen (1982)] is employed to obtain this limiting value of the stress intensity factor from its value for a standing crack in an elastic material with the same geometry and boundary conditions. Beginning with the result for the standing crack in (42), it is possible to show for two bonded Maxwell materials that

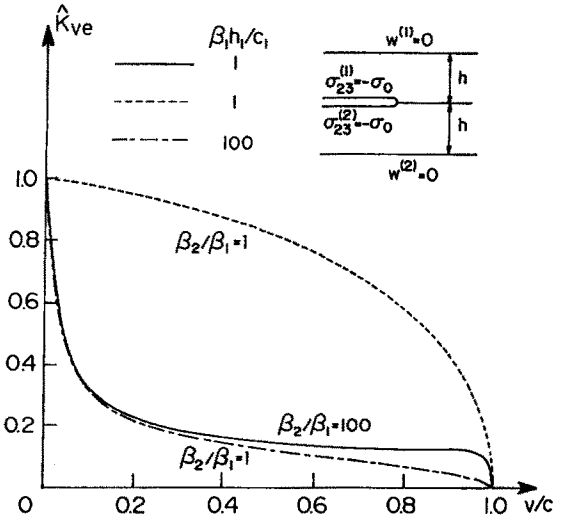

Fig. 4. Graph of the non-dimensional stress intensity factor $\hat{K}_{ve}$ vs the non-dimensional crack-tip velocity v/c for an inhomogeneous viscoelastic (Maxwell material) strip with $\mu_2/\mu_1 = 1$, $c_2/c_1 = 1$, $h_2/h_1 = 1$, $\beta_2/\beta_1 = 100$ (solid line). The other two curves are homogeneous viscoelastic strips from Fig. 3.

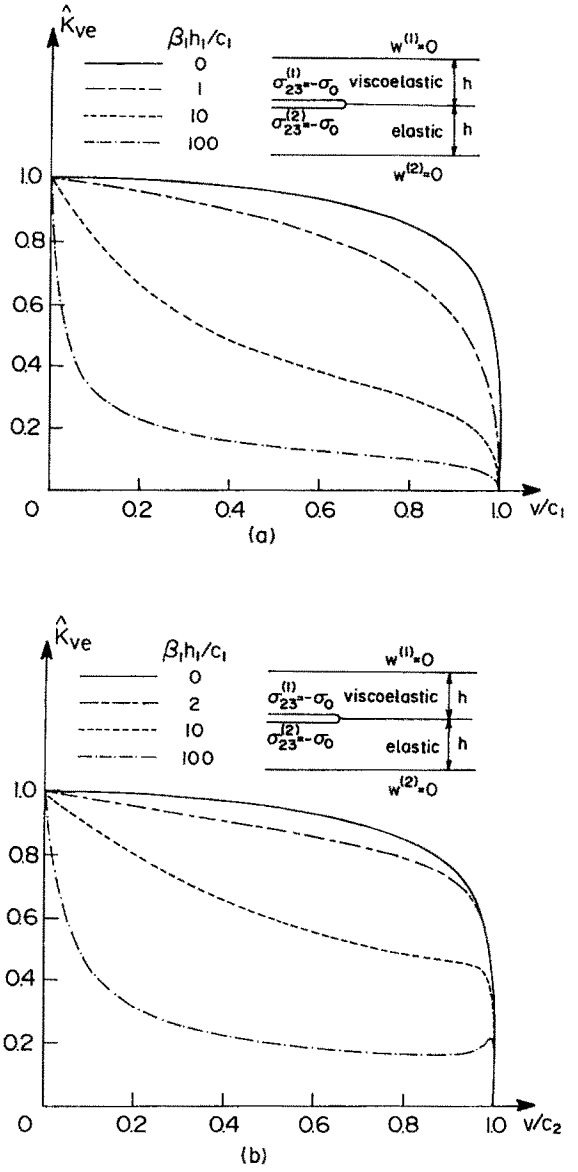

Fig. 5. Graph of the non-dimensional stress intensity factor $\hat{K}_{ve}$ for a bonded viscoelastic (Maxwell material) and elastic strip with a crack along the interface and $h_2/h_1 = 1$, $\mu_2/\mu_1 = 1$. The shear wave speeds are unequal with (a) $c_2/c_1 = 2$ and (b) $c_2/c_1 = 0.5$.

$$\hat{K}_{ve}^0 = \left[\frac{\left(1+\frac{\mu_2}{\mu_1}\right)\left(\frac{h_2}{h_1}\frac{\beta_2}{\beta_1}+\frac{\mu_2}{\mu_1}\right)}{\left(\frac{h_2}{h_1}+\frac{\mu_2}{\mu_1}\right)\left(\frac{\beta_2}{\beta_1}+\frac{\mu_2}{\mu_1}\right)} \right]^{1/2} . \tag{52}$$

It may be noted that the parameters c_2/c_1 and $\beta_1 h_1/c_1$ do not appear in (52) and, hence, do not influence the value of $\hat{K}_{ve}$ at $v = 0$. Further, for a homogeneous strip, $\hat{K}_{ve}^0$ is unity. For an inhomogeneous strip composed of two Maxwell materials in which either the thickness of each material or their relaxation times are identical, again $\hat{K}_{ve}^0$ is unity. This result contrasts with that determined by Sills and Benveniste (1981) for two bonded half-spaces, each a Maxwell material with a steadily propagating mode III crack between them. In that study, the non-dimensional stress intensity factor is unity at $v = 0$ for all combinations of

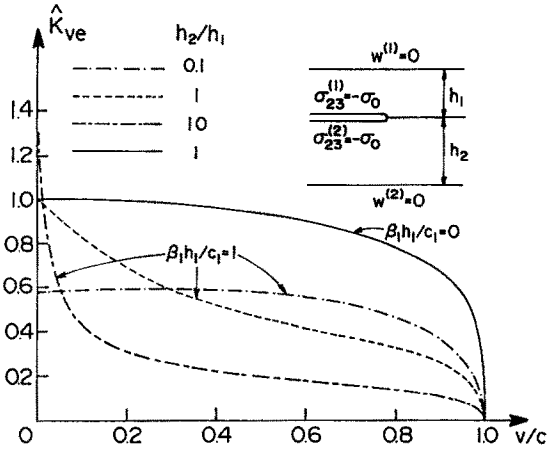

Fig. 6. Graph of the non-dimensional stress intensity factor $\hat{K}_{ve}$ vs the non-dimensional crack-tip velocity v/c for inhomogeneous viscoelastic (Maxwell material) composites with $\mu_2/\mu_1 = 1$, $c_2/c_1 = 1$, $\beta_1 h_1/c_1 = 1$ and $\beta_2/\beta_1 = 10$. The effect of various h_2/h_1 ratios are compared. Also shown are results for a homogeneous elastic strip (solid line).

material parameters. In each case considered below, for small v, the numerically obtained values of the stress intensity factor are seen to approach the value of $\hat{K}_{ve}^0$ in (52).

On the other hand, at $v = \min(c_1, c_2)$, the rate of convergence of J in (40) decreases. It may be observed however, from (A11) that the integrand and hence J is negative. Consequently, the exponential in (43) is bounded. Moreover, the coefficient of this exponential goes to zero at $v = \min(c_1, c_2)$. This may be seen by noting that either a_1 or a_2 of (27) is zero at this value of v, causing the denominator of the coefficient of $\exp(J)$ to become infinite. Hence, $\hat{K}_{ve}$ tends to zero as v approaches $\min(c_1, c_2)$.

In Fig. 3, results are first presented for a homogeneous, viscoelastic strip in which $h \equiv h_1 = h_2$. The non-dimensional stress intensity factor $\hat{K}_{ve}$ is shown versus the non-dimensional velocity. In this case, $c \equiv c_1 = c_2$, $\beta \equiv \beta_1 = \beta_2$, and the shear moduli are equal. From this figure, it is possible to examine the influence of the ratio of a strip wave travel time to the relaxation time $\beta h/c$, on the stress intensity factor in a homogeneous strip. Four values of $\beta h/c$ are chosen to study this effect, from elastic with $\beta h/c = 0$ to strongly viscoelastic $\beta h/c = 100$. The elastic result is taken from Sih and Chen (1977) and shown as

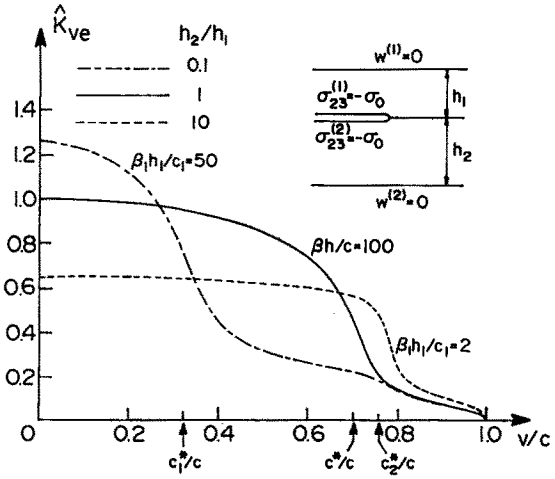

Fig. 7. Graph of the non-dimensional stress intensity factor $\hat{K}_{ve}$ vs the non-dimensional crack-tip velocity v/c for bonded standard solid composites with $\mu_2/\mu_1 = 1$, $c_2/c_1 = 1$, $\beta_2/\beta_1 = 10$, $\alpha_2/\alpha_1 = 60$, $\alpha_1/\beta_1 = 0.1$. Also shown are results for a homogeneous standard solid strip (solid line) with $\alpha/\beta = 1/2$ and $\beta h/c = 100$.

the solid line. The stress intensity factor decreases monotonically from its value of unity at $v/c = 0$ to zero at $v/c = 1$. As the relaxation time decreases, i.e. as $\beta h/c$ increases, the stress intensity factor decreases more rapidly as v increases. Until, when $\beta h/c = 100$, it drops off precipitously at small values of v/c. It may be noted that to the authors' knowledge, graphical results for a homogeneous strip composed of a Maxwell material do not appear in the literature.

In Fig. 4, two of the curves for homogeneous viscoelastic strips presented in Fig. 3 are repeated for comparison to an inhomogeneous strip. For this latter case, the crack is positioned symmetrically with respect to the two materials ($h_2/h_1 = 1$), and the shear moduli and wave speeds are taken equal, so that $\mu_2/\mu_1 = 1$, $c \equiv c_1 = c_2$. The ratio of the relaxation times $\beta_2/\beta_1 = 100$ and $\beta_1 h_1/c_1 = 1$. The $\hat{K}_{ve}$ values for this case are between those of the two homogeneous strips. For small crack-tip velocities, both constituents have "time to relax" and hence the strip behaves like a homogeneous viscoelastic strip with a short relaxation time. For crack-tip velocities approaching the shear wave speed, the constituents do not have sufficient time to relax; so that, $\hat{K}_{ve}$ values increase locally, approaching those of the homogeneous strip whose behavior is similar to that of an elastic strip (see Fig. 3).

Next, the case of a crack between a bonded viscoelastic and elastic strip is presented in Figs 5(a) and (b). In these figures, the effect of the ratio c_2/c_1 is examined. For all material combinations presented, the crack is located symmetrically with respect to the two materials or $h_2/h_1 = 1$ and the shear modulus ratio $\mu_2/\mu_1 = 1$. In Fig. 5(a), $c_2/c_1 = 2$, so that the non-dimensional velocity is v/c_1. The parameter $\beta_1 h_1/c_1$ varies between zero and 100, or from an elastic strip with two constituents of different densities to a bonded elastic/viscoelastic strip where the relaxation time of the viscoelastic material is relatively small. Analogous behavior may be observed in comparing Fig. 5(a) with Fig. 3 for a homogeneous viscoelastic strip; that is, for $c_2/c_1 > 1$, the qualitative behavior of the stress intensity factor for the homogeneous and inhomogeneous strip, with one constituent elastic, is similar. Note that the smaller wave speed is associated with the viscoelastic medium. On the other hand, in Fig. 5(b) $c_2/c_1 = 1/2$. Here, the elastic medium has a shear wave speed smaller than that of the viscoelastic medium and the non-dimensional velocity is v/c_2. For v approaching c_2, the stress intensity factor "attempts" to behave like the elastic material or the material with the smaller wave speed. It appears that for v close to the min (c_1, c_2), the behavior of the stress intensity factor is dominated by the material with the smaller shear wave speed.

In Fig. 6, the influence of crack position within the inhomogeneous viscoelastic strip on the stress intensity factor is examined. For comparison, results for a homogeneous elastic strip are also presented (solid line). The shear modulus ratio μ_2/μ_1 and the parameter $\beta_1 h_1/c_1$ are taken to be unity; the shear wave speeds are equal, $c \equiv c_1 = c_2$; the ratio of relaxation times $\beta_2/\beta_1 = 10$. Three thickness ratios are considered: $h_2/h_1 = 0.1, 1, 10$. This graph differs from the previous ones in that the value of the stress intensity factor $\hat{K}_{ve}$ for crack tip speed $v = 0$ does not approach unity. This may be confirmed by use of eqn (52). For the parameters chosen, $\hat{K}^0_{ve} > 1$ when the relaxation time of the thinner strip is greater than that of the thicker strip. It may be noted that for $v/c \gtrsim 0.4$, for the thickness combinations presented, the nondimensional stress intensity factor is significantly smaller than that for an elastic homogeneous material. For small crack tip velocities, the stress intensity values are quite different. This result may be of some practical importance. It indicates that the stress intensity factor of a crack strip may be significantly lowered for small crack speeds (as much as 40%, in this case) by bonding a thin strip whose relaxation time is smaller than that of the second Maxwell material.

3.2. *Standard solid*

For a bi-material, standard solid strip, several additional non-dimensional parameters are required so that

$$\hat{K}_{ve} = \hat{K}_{ve}[v/\min(c_1, c_2); \alpha_2/\alpha_1, \alpha_1/\beta_1, \beta_2/\beta_1, \beta_1 h_1/c_1, h_2/h_1, c_2/c_1, \mu_2/\mu_1]. \tag{53}$$

At $v = 0$, it is possible to show by means of the correspondence principle that

$$\hat{K}_{ve}^{0} = \left[\frac{\left(1+\frac{\mu_2}{\mu_1}\right)\left(\frac{h_2}{h_1}+\frac{\mu_2^*}{\mu_1^*}\right)}{\left(\frac{h_2}{h_1}+\frac{\mu_2}{\mu_1}\right)\left(1+\frac{\mu_2^*}{\mu_1^*}\right)} \right]^{1/2}. \tag{54}$$

This limiting value of the stress intensity factor will be unity when the crack is centrally located or when the ratios of relaxation and creep times are equal, namely $\alpha_2/\alpha_1 = \beta_2/\beta_1$. For other cases near $v = 0$, behavior similar to that seen in Fig. 6 for Maxwell materials will occur. The limiting behavior at $v = \min(c_1, c_2)$ is more difficult to determine than in the case of Maxwell materials where the integrand in (40) is negative for $t > 0$. For two bonded, standard solids, it may be shown that the integrand in (40) is negative for all values of t greater than some t_0 which is independent of a_r. Thus, the exponential in (39) is bounded and as with the Maxwell material, $\hat{K}_{ve}$ approaches zero as v approaches the smaller of the short time shear wave speeds. In addition, it is possible to rewrite the non-dimensional stress intensity factor $\hat{K}_{ve}^{0}$ as

$$\hat{K}_{ve}^{0} = \frac{K_e^*}{K_e}, \tag{55}$$

where the elastic stress intensity factor K_e is given in (42) and K_e^* may be thought of as the stress intensity factor of a bi-material, elastic strip whose shear moduli are the long time moduli u_r^*.

Indeed, the general behavior of the non-dimensional stress intensity factor changes somewhat in that it is now influenced by the long time wave speeds $c_r^{*2} = \alpha_r c_r^2/\beta_r = \mu_r^*/\rho_r$. As opposed to the behavior observed for a semi-infinite crack running steadily between two half-spaces composed of two standard solids (Banks-Sills and Benveniste, 1983), the slope of the curves in Fig. 7 for two bonded standard solid strips is seen to be continuous. This was also observed in the study by Atkinson and Popelar (1979) in which they considered a homogeneous, standard solid strip. Results from their work are reproduced and shown as the solid curve in Fig. 7, as well. For this curve, all parameter ratios in (53) are unity except for $\alpha/\beta = 1/2$ and $\beta h/c = 100$. It may be observed that the non-dimensional stress intensity factor decreases slowly until $v/c = c^*/c = \sqrt{2}/2$, where it decreases precipitously. These results for this curve were determined by equations presented in this investigation. They coincide with those presented by Atkinson and Popelar (1979).

The two other curves presented in Fig. 7 are for composite strips whose constituents are standard solids. The parameters for both cases are $\alpha_2/\alpha_1 = 60$, $\alpha_1/\beta_1 = 0.1$, $\beta_2/\beta_1 = 10$ and $c_2/c_1 = \mu_2/\mu_1 = 1$; the long time wave speeds are $c_1^*/c = \sqrt{0.1}$ and $c_2^*/c = \sqrt{0.6}$ ($c = c_1 = c_2$) and the long time modulus ratio is $\mu_2^*/\mu_1^* = 6$. In one case, the thickness ratio is $h_2/h_1 = 0.1$ and $\beta_1 h_1/c_1 = 50$; whereas, in the second case, $h_2/h_1 = 10$ and $\beta_1 h_1/c_1 = 2$. As may be seen from (54) and Fig. 7, the strip thickness ratio has a strong influence on the non-dimensional stress intensity factor for small and intermediate crack-tip speeds. For $v = 0$, $\hat{K}_{ve}^{0} > 1$ when $\mu_2^*/\mu_1^* < \mu_2/\mu_1$ and $h_2 > h_1$. For non-dimensional crack-tip speed near c_1^*/c, the slope of the curve describing the stress intensity factor behavior changes rapidly for the composite whose thick constituent is associated with this long time wave speed (i.e. the upper material, $h_2/h_1 = 0.1$). On the other hand for $h_2/h_1 = 10$, when v/c is near c_2^*/c, the slope of the other curve changes rapidly. In this case again, the thicker strip is associated with this long time wave speed. The alternative curves have small changes in slope at these points. It may be further noted that in calculating the stress intensity factor for these various cases, the same expression given in (43) is employed for all values of crack-tip velocity v. However, as is mentioned in the Appendix, the validation of condition (c) is carried out numerically for $v > c_r^*$.

4. CONCLUSIONS

A non-dimensional stress intensity factor for a steadily propagating, interface, mode III crack in a bonded strip composed of two viscoelastic solids has been determined. The

materials were modeled as Maxwell materials and standard solids. The stress intensity factor was expressed in non-dimensional parameters and the effect of several of these was examined.

For a homogeneous Maxwell material, the non-dimensional stress intensity factor decreases more rapidly for increasing crack-tip velocity as the relaxation time decreases. For an inhomogeneous strip composed of two Maxwell materials, in which there is a great difference between their relaxation times, the non-dimensional stress intensity factor decreases rapidly at small crack-tip speeds. For an elastic strip bonded to a Maxwell material, the behavior is quite similar to that of a homogeneous Maxwell material. When the wave speed of the elastic material is smaller than that of the viscoelastic material, the non-dimensional stress intensity factor approaches that of a homogeneous elastic strip for values of the crack-tip velocity which approach that speed. It is further observed that the relative strip thickness of two Maxwell materials is important at small crack-tip velocities. Bonding of a thin viscoelastic strip significantly lowers the stress intensity factor as compared to that of a homogeneous strip. For two standard solids, the behavior of the non-dimensional stress intensity factor is similarly affected by the individual strip thicknesses. In addition, the long time wave speeds c_r^* influence this behavior in a manner similar to that of a homogeneous strip with the thicker layer dominating the behavior.

Acknowledgement—This work was supported in part by the Ministry of Immigrant Absorption, Israel. Other parts of this work were carried out in the Eda and Jaime David Dreszer Fracture Mechanics Laboratory, Faculty of Engineering, Tel Aviv University.

REFERENCES

Atkinson, S. and Popelar, C. H. (1979). Antiplane dynamic crack propagation in a viscoelastic strip. *J. Mech. Phys. Solids* **27,** 431–439.

Banks-Sills, L. and Benveniste, Y. (1983). Steady interface crack propagation between two viscoelastic standard solids. *Int. J. Fract.* **21,** 243–260.

Christensen, R. M. (1982). *Theory of Viscoelasticity*. Academic Press, New York.

Coussy, O. (1987). A moving crack problem along the interface of two viscoelastic media. *Int. J. Engng Sci.* **25,** 609–620.

Gakhov, F. D. (1966). *Boundary Value Problems* (translated from Russian). Pergamon Press, London.

Matczynski, M. (1974). Quasistatic problem of a non-homogeneous elastic layer containing a crack. *Acta Mech.* **19,** 153–168.

Noble, B. (1958). *The Wiener–Hopf Technique*. Pergamon Press, London.

Sih, G. C. and Chen, E. P. (1977). Cracks moving at constant velocity and acceleration. In *Mechanics of Fracture* (Edited by G. C. Sih), Vol. 4, pp. 59–117. Noordoff, Leyden.

Sills, L. B. and Benveniste, Y. (1981). Steady state propagation of a mode III interface crack between dissimilar viscoelastic media. *Int. J. Engng Sci.* **19,** 1255–1268.

Walton, J. R. (1985). The dynamic steady-state propagation of an antiplane shear crack in a general linearly viscoelastic layer. *J. Appl. Mech.* **52,** 853–856.

APPENDIX

In the Appendix, condition (c) required for factorization of $F_2(s)$ in eqn (22) is verified for both a pair of Maxwell materials and standard solids.

First, for the Maxwell materials, mapping of contour L by $F_2(s)$ in eqn (20) is examined. It may be recalled that the expression $\tanh(\gamma_r h_r)/\mu_r\gamma_r$ is meromorphic. Therefore from its definition in eqn (29), $F_2(s)$ has neither poles nor zeros in a sufficiently small neighborhood of the real axis, $\mathrm{Im}(s) = 0$. Thus, the indices $F_2(s)$ on L and on the real axis L_1 are equal. It is then possible to more conveniently determine the index of $F_2(s)$ on L_1.

The mapping of L_1 by $F_2(s)$ is defined as $\tilde{L}_1$. Satisfaction of condition (b) and continuity of $F_2(s)$ on L_1, guarantees that $\tilde{L}_1$ is a closed contour. Demonstration that the index of $F_2(s)$ is zero on L_1 is equivalent to showing that $\tilde{L}_1$ does not encircle the origin of the mapped plane. First of all, it may be shown that $\tilde{L}_1$ is symmetric with respect to the real axis, namely $\mathrm{Im}[F_2(s)] = 0$. This follows from the symmetric property

$$\Psi(-\tau) = \bar{\Psi}(\tau), \quad \tau = \mathrm{Re}(s), \tag{A1}$$

which is fulfilled by $\gamma_r^2(s)$ in (26), $P(s)$ in (28) and hence $F_2(s)$ in (29). Next, since

$$F_2(0) = \frac{Q(0)}{Q(\infty)}, \tag{A2}$$

where

$$Q(0) = \frac{h_1}{\mu_1} + \frac{\beta_2}{\beta_1}\frac{h_2}{\mu_2} \tag{A3}$$

and $F_2(\infty) = 1$, $F_2(\tau)$ is real and positive, for $\tau = 0$ and ∞. Finally, it must be shown that

$$\arg F_2(\tau) \neq -\pi, \quad 0 < \tau < \infty. \tag{A4}$$

To this end, the range of the arguments of each of the functions constituting $F_2(s)$ in (29) is determined below. First, $\gamma_r(s)$ is considered. Since s^2 is real for s real, the argument of $\gamma_r^2(s)$ in (26) is equal to the argument of $\gamma_r^2(s)/s^2$. This latter function represents a bilinear transformation which maps the real axis into a straight line, namely $\mathrm{Re}\,[\gamma_r^2(s)/s^2] = a_r^2$. As may be recalled, the branch of γ_r was chosen with $\mathrm{Re}\,(\gamma_r) > 0$, so that

$$0 < \arg \gamma_r(\tau) < \frac{\pi}{4}, \quad 0 < \tau < \infty. \tag{A5}$$

Moreover, for a complex variable z with $0 < \arg z < \pi/2$,

$$|\arg (\tanh z)| < \frac{\pi}{4}, \tag{A6}$$

and

$$\mathrm{Im}\left(\frac{\tanh z}{z}\right) < 0. \tag{A7}$$

Since the range of $\arg (\gamma_r h_r)$ is more restricted by (A5) than that of z, one may immediately observe from (A5)–(A7) that

$$-\frac{\pi}{2} < \arg\left(\frac{\tanh (\gamma_r h_r)}{\gamma_r h_r}\right) < 0, \quad 0 < \tau < \infty. \tag{A8}$$

Now, the function defined by

$$f_1(s) = \frac{s - i\beta_2/v}{s - i\beta_1/v} \tag{A9}$$

maps the real axis L_1, onto a circle in the right half of the mapped plane which is symmetric with respect to the axis $\mathrm{Im}\,[f_1(s)] = 0$. Without loss of generality, choosing $\beta_2 > \beta_1$, it is clear that

$$-\frac{\pi}{2} < \arg f_1(\tau) < 0, \quad 0 < \tau < \infty.$$

Hence,

$$-\pi < \arg\left\{f_1(s)\left(\frac{\tanh (\gamma_2 h_2)}{\gamma_2 \mu_2}\right)\right\} < 0, \quad 0 < \tau < \infty. \tag{A10}$$

From (29), (A8) and (A10), it is then possible to conclude that

$$-\pi < \arg F_2(\tau) < 0, \quad 0 < \tau < \infty \tag{A11}$$

so that the relation in (A4) is satisfied.

From the symmetry of $\tilde{L}_1$, the fact that $F_2(\tau)$ is real and positive for $\tau = 0$ and ∞ and the inequality in (A4), it is clear that $\tilde{L}_1$ does not encircle the origin. Thus, condition (c) is verified for two Maxwell materials and $F_2^{\pm}(s)$ may be determined from the integral in (22).

Next, for two standard solids, all conditions mentioned in the previous paragraph for the Maxwell material are easily demonstrated except for relation (A4). This is shown now. Note that each of the functions $\psi_r(s)$ in (46) represents a bilinear transformation which maps the real axis into a circle situated in the right half of the mapped plane. As with $f_1(s)$ in (A9), it may be shown that

$$-\frac{\pi}{2} < \arg \psi_r(\tau) < 0, \quad 0 < \tau < \infty. \tag{A12}$$

The range of angles in (A12) results from the well-known relation for standard solids, $\beta_r > \alpha_r$. Next, $\gamma_r(s)$ in (13) requires consideration. The function $\gamma_r^2(s)/s^2$ represents a bilinear transformation, as in the previous case, which

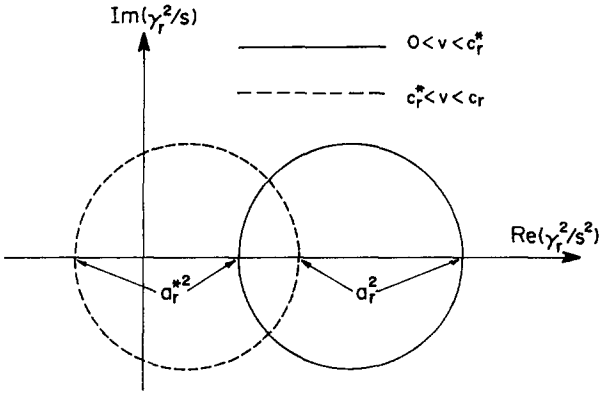

Fig. A1. Mapping of the real axis L_1 by the function γ_r^2/s^2 for two ranges of crack tip velocity v.

maps the real axis L_1, onto a circle as illustrated in Fig. A1. The position of the circle depends upon the relationship between the magnitude of the crack-tip velocity v and the long time wave speed c_r^*. Without loss of generality, the long time wave speed of the upper material is chosen smaller than that of the lower material, namely $c_1^* < c_2^*$. If c_1 is less than c_2^*, the behavior of γ_r changes within the regions: (i) $0 < v < c_1^*$ and (ii) $c_1^* < v < c_1$. If on the other hand, c_1 is greater than c_2^* there are three regions, namely (i) $0 < v < c_1^*$, (ii) $c_1^* < v < c_2^*$ and (iii) $c_2^* < v < \min(c_1, c_2)$. First, the possibility of two different regions is considered; afterwards, the second alternative is addressed

Case (i) $0 < v < c_1^*$

In this region,

$$\left.\frac{\gamma_r^2(s)}{s^2}\right|_{s=0} = a_r^{*2} > 0,$$

where

$$a_r^{*2} = 1 - v^2/c_r^{*2}.$$

Therefore, for the chosen branch of γ_r with $\mathrm{Re}(\gamma_r) > 0$, relation (A5) for $\arg(\gamma_r)$ and, consequently, (A8) remain valid. It may be immediately observed from (45) and (A12), that relation (A11) is fulfilled and the desired inequality (A4) is satisfied; so that, condition (c) is verified for this case.

Case (ii) $c_1^* < v < c_1$

In this region, $a_1^* < 0$, so that the circle representing the mapped real axis crosses the imaginary axis as shown in Fig. A1. As a result, instead of (A5)

$$0 < \arg \gamma_1(\tau) < \frac{\pi}{2}, \quad 0 < \tau < \infty. \tag{A13}$$

For $\gamma_2(\tau)$, relation (A5) remains valid. No attempt is made to analytically verify condition (c). In this case, condition (c) is verified numerically for each set of material parameters. This may be carried out easily when calculating stress intensity factors.

If $c_1 > c_2^*$, case (i) is the same as above. Verification of condition (c) may be carried out numerically for cases (ii) and (iii).